PHYSICAL REVIEW B **77**, 134412 (2008)

Disordered ground states in a quantum frustrated spin chain with side chains

Ken'ichi Takano[1] and Kazuo Hida[2]
[1]*Toyota Technological Institute, Tenpaku-ku, Nagoya 468-8511, Japan*
[2]*Division of Material Science, Graduate School of Science and Engineering, Saitama University, Saitama 338-8570, Japan*
(Received 15 October 2007; revised manuscript received 29 February 2008; published 3 April 2008)

We study a frustrated mixed spin chain with side chains, where the spin species and the exchange interactions are spatially varied. A nonlinear σ model method is formulated for this model, and a phase diagram with two disordered spin-gap phases is obtained for typical cases. Among them, we examine the case with a main chain, which consists of an alternating array of spin-1 and spin-$\frac{1}{2}$ sites, and side chains, each of which consists of a single spin-$\frac{1}{2}$ site, in great detail. Based on numerical, perturbational, and variational approaches, we propose a singlet cluster solid picture for each phase, where the ground state is expressed as a tensor product of local singlet states.

DOI: 10.1103/PhysRevB.77.134412 PACS number(s): 75.10.Jm, 75.10.Pq, 75.30.Et, 75.30.Kz

I. INTRODUCTION

Quantum one-dimensional (1D) spin systems have been studied in various aspects, with particular interest in their strong quantum fluctuations due to the low dimensionality. There appear a variety of quantum disordered ground states where the continuous spin rotation symmetry is not broken and the lowest spin excitation has a finite gap (spin gap). These quantum disordered states have no analogs in classical spin systems. Typical examples are a Haldane state in a spin-1 chain,[1] a dimer state in a spin-$\frac{1}{2}$ chain with bond alternation,[2] and a spin-gap state in a spin-$\frac{1}{2}$ ladder.[3]

In extensive research for various 1D spin systems, spin chains with side chains have not attracted enough attention in spite of their potentially rich physics. Since a side chain is of finite length, it may enhance quantum fluctuation in the system. Actually, the 1D Kondo necklace model, which has been extensively studied as a simplified version of the 1D Kondo lattice model,[4,5] can be regarded as a spin chain with side chains. In this model, the main chain is a spin-$\frac{1}{2}$ chain and each side chain consists of a single spin with magnitude of $\frac{1}{2}$. The ground state of this model is known to be in the Kondo singlet phase with spin gap,[5] while the spin-$\frac{1}{2}$ chain without side chains is critical. This means that the quasi-long-range order in the main chain is destroyed by the quantum fluctuation in the side chains. Also, if the side chains bring geometrical frustration into the system, quantum fluctuation is expected to be further enhanced. Thus, how quantum fluctuation manifests itself and what kind of ground state appears in various types of spin chains with side chains are interesting subjects.

In this paper, we investigate the nature of quantum disordered ground states of one of the simplest models with frustrated side chains. The main chain of the model consists of two species of spins in alternating order, and each side chain consists of a single spin, with each side chain alternately attached to the main chain, as shown in Fig. 1. This model incorporates the effects of a mixture of different spins, bond alternation, and frustration in spite of its simplicity. In particular, the frustration comes from triangles, each consisting of three antiferromagnetically interacting spins. Although quantum spin systems with similar geometry have been investigated by several authors,[6] our model is physically different from them. If the side chains of our model are removed, the main chain is in a ferrimagnetic ground state. The side-chain spins introduce frustration to the system and destroy the ferrimagnetic order, leading to quantum disordered states.

The disordered ground states of the present model cannot be understood in the conventional valence bond solid (VBS) picture,[7] which successfully explains the disordered ground states of many spin models with local frustration. Instead, we will explain the present ground states using the concept of the singlet cluster solid (SCS) picture. A SCS state is a direct product of local singlet states or singlet clusters. Each singlet cluster consists of more than two singlet dimers, and the dimers are resonating locally within the cluster. The SCS states are realized as a result of the interplay of quantum fluctuation and local frustration, as will be explained in detail.

It is desirable that the SCS state manifested in this paper is experimentally inspected in materials. However, a material precisely described by the present model has not been found so far to our knowledge. Despite the lack of materials, it is worth clarifying the concept of the SCS states and verifying their existence in a concrete model. Further, by considering the rich variety of magnetic materials synthesized by modern chemical technology,[8] desired materials are expected to be synthesized, since they are not necessarily complex in structure.

The details of the model are explained in the next section. Various approaches are employed to clarify the ground-state phases of this model. In Sec. III, a nonlinear σ model

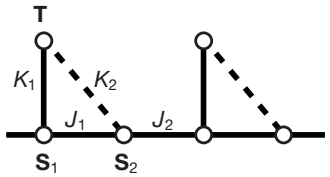

FIG. 1. A quantum spin chain with side chains; two unit cells are presented. $\mathbf{S}_1$, $\mathbf{S}_2$, and $\mathbf{T}$ are spins whose magnitudes satisfy Eq. (3). The case where $S_1=1$, $S_2=\frac{1}{2}$, and $T=\frac{1}{2}$ is particularly studied in detail.

(NLSM) method is proposed to grasp a qualitative feature of the phase diagram. Since a similar NLSM method has been developed for mixed spin chains without side chains, we extend it to the present side-chain case.

We also employ other approaches while limiting ourselves to the simplest cases of spin magnitudes of 1 and $\frac{1}{2}$. In Sec. IV, a numerical diagonalization for finite systems is carried out to obtain a quantitatively reliable phase diagram, which confirms the qualitative correctness of the NLSM method. Some limiting cases are exactly treated to draw a physical picture for each phase in Sec. V. After these considerations, we arrive at the SCS pictures to explain the ground states in Sec. VI. The SCS pictures are also supported by variational calculations in Sec. VII. Section VIII is devoted to a summary and discussion.

II. MODEL HAMILTONIAN AND ITS CLASSICAL VERSION

We study an isotropic quantum spin chain with alternately arrayed side chains, as illustrated in Fig. 1. In the pth unit cell, $\mathbf{S}_1(p)$ and $\mathbf{S}_2(p)$ are spin operators on the main chain, and $\mathbf{T}(p)$ is a spin operator on the side chain. The quantum numbers of spin magnitudes of these spin operators are expressed as S_1, S_2, and T. Exchange parameters are represented as J_1, J_2, K_1, and K_2 and are assumed to be all positive. Then the Hamiltonian is written as

$$H = \sum_{p=1}^{N} \{J_1 \mathbf{S}_1(p) \cdot \mathbf{S}_2(p) + J_2 \mathbf{S}_2(p) \cdot \mathbf{S}_1(p+1) + K_1 \mathbf{S}_1(p) \cdot \mathbf{T}(p) + K_2 \mathbf{S}_2(p) \cdot \mathbf{T}(p)\}. \quad (1)$$

The spacing between the nearest spins is a, and the length of a unit cell is $2a$. The Hamiltonian is characterized by three independent dimensionless parameters, as follows:

$$j = \frac{J_2}{J_1}, \quad k = \frac{TK_1}{S_2 J_1}, \quad r = \frac{S_2 K_2}{S_1 K_1}. \quad (2)$$

Here, j measures the strength of the bond alternation in the main chain, k measures the strength of interaction between a main-chain spin and a side-chain spin, and r measures the strength of frustration.[9]

In the present paper, we assume the following restriction on spin magnitudes:

$$S_1 - S_2 - T = 0. \quad (3)$$

This is the condition that the corresponding classical spin chain can have a ground state with no total magnetization (i.e., no ferrimagnetism) when K_2 is not large. The restriction (3) serves to simplify the Berry phase term in the continuum limit.

Expectation values of the spin operators for a spin coherent state are written as

$$\langle \mathbf{S}_1(p) \rangle = S_1 \mathbf{M}_1(p),$$

$$\langle \mathbf{S}_2(p) \rangle = -S_2 \mathbf{M}_2(p),$$

$$\langle \mathbf{T}(p) \rangle = -T \mathbf{M}_\perp(p), \quad (4)$$

where $\mathbf{M}_1(p)$, $\mathbf{M}_2(p)$, and $\mathbf{M}_\perp(p)$ are unit vectors. By substituting them for the spin operators in Eq. (1), we have the following classical version of the Hamiltonian:

$$H_c = \frac{1}{2}\tilde{J}_1 \sum_{p=1}^{N} \left\{ j[\mathbf{M}_2(p) - \mathbf{M}_1(p+1)]^2 + \left(1 - \frac{kr}{1-r}\right)[\mathbf{M}_1(p) - \mathbf{M}_2(p)]^2 + \frac{k}{1-r}[\mathbf{M}_1(p) - r\mathbf{M}_2(p) - (1-r)\mathbf{M}_\perp(p)]^2 \right\}, \quad (5)$$

where $\tilde{J}_1 = J_1 S_1 S_2$ and a constant term is omitted from H_c. The classical antiferromagnetic configuration,

$$\mathbf{M}_1(p) = \mathbf{M}_2(p') = \mathbf{M}_\perp(p'') \quad (6)$$

for all p, p', and p'', is the ground-state solution if the prefactors of the squares in Eq. (5) are all positive. This gives the condition for the classical stability of the antiferromagnetism as

$$0 < r < 1, \quad 0 < k < \frac{1}{r} - 1. \quad (7)$$

In the following arguments, we will concentrate on this region.

III. NONLINEAR σ MODEL FOR THE SPIN CHAIN

By using the spin coherent representation, the partition function of Hamiltonian (1) is written in a path-integral form as

$$Z = \int \prod_j D[\mathbf{M}_j] \delta(\mathbf{M}_j^2 - 1) e^{-A}, \quad (8)$$

with $j = 1$, 2, and $\perp$. The action A is written as

$$A = -iA_B + A_H,$$

$$A_B = \sum_p \{S_1 w[\mathbf{M}_1(p)] - S_2 w[\mathbf{M}_2(p)] - T w[\mathbf{M}_\perp(p)]\},$$

$$A_H = \int_0^\beta d\tau H_c, \quad (9)$$

where β is the inverse of temperature and $w[\mathbf{M}_i(p)]$ is the solid angle that $\mathbf{M}_i(p)$ forms in period β. The term $-iA_B$ in action A is the Berry phase term.

We introduce a slow variable $\mathbf{m}(p)$ for each unit cell and fluctuation variables $\mathbf{L}_1(p)$, $\mathbf{L}_2(p)$, and $\mathbf{L}_\perp(p)$ for each spin in a unit cell. Then the original variables are transformed as follows:

$$\mathbf{M}_1(p) = \mathbf{m}(p) + a\mathbf{L}_1(p),$$

$$\mathbf{M}_2(p) = \frac{1}{2}\mathbf{m}(p) + \frac{1}{2}\mathbf{m}(p+1) + a\mathbf{L}_2(p),$$

$$\mathbf{M}_\perp(p) = \mathbf{m}(p) + a\mathbf{L}_\perp(p). \tag{10}$$

This transformation is found by observing and extending the transformation for a simple chain without a side chain.[10,11] Since the left hand side terms in Eq. (10) are unit vectors, we have the following constraints for the new variables:

$$\mathbf{m}^2 = 1, \quad \mathbf{m}\cdot\mathbf{L}_1 = \mathbf{m}\cdot\mathbf{L}_2 = \mathbf{m}\cdot\mathbf{L}_\perp = 0. \tag{11}$$

The fluctuation variables depend on one another, and one of them, e.g., $\mathbf{L}_\perp$, can be set equal to 0. Hence, the number of independent variables is conserved in the transformation. By defining new fluctuation variables,

$$\mathbf{R} = \mathbf{L}_2 - \mathbf{L}_1,$$

$$\mathbf{Q} = (1-r)\mathbf{L}_\perp - \mathbf{L}_1 + r\mathbf{L}_2, \tag{12}$$

and taking the continuum limit, we have

$$A = \int d\tau dx \left\{ \frac{i}{2} S_2 \frac{\partial \mathbf{m}}{\partial x} \cdot \left(\mathbf{m} \times \frac{\partial \mathbf{m}}{\partial \tau} \right) + \frac{a}{4}\tilde{J}_1 (c_+ - kr^2) \left(\frac{\partial \mathbf{m}}{\partial x} \right)^2 + \frac{a}{4}\tilde{J}_1 [k(\mathbf{Q}^2 + 2\mathbf{f}\cdot\mathbf{Q}) + c_+(\mathbf{R}^2 + 2\mathbf{g}\cdot\mathbf{R})] \right\}, \tag{13}$$

with $c_\pm = 1 \pm j - [kr/(1-r)]$. Here, vectors $\mathbf{f}$ and $\mathbf{g}$ are given as

$$\mathbf{f} = r\frac{\partial \mathbf{m}}{\partial x} + i\frac{S_1 - S_2}{a\tilde{J}_1 k(1-r)} \mathbf{m} \times \frac{\partial \mathbf{m}}{\partial \tau},$$

$$\mathbf{g} = \frac{c_-}{c_+}\frac{\partial \mathbf{m}}{\partial x} - i\frac{rS_1 - S_2}{c_+ a\tilde{J}_1 (1-r)} \mathbf{m} \times \frac{\partial \mathbf{m}}{\partial \tau}. \tag{14}$$

By integrating the partition function with respect to $\mathbf{R}$ and $\mathbf{Q}$, we have the following NLSM action:

$$A_{\text{eff}} = \int d\tau \int dx \left\{ i\frac{\theta}{4\pi} \mathbf{m} \cdot \left(\frac{\partial \mathbf{m}}{\partial \tau} \times \frac{\partial \mathbf{m}}{\partial x} \right) + \frac{c_+(S_1 - S_2)^2 + k(rS_1 - S_2)^2}{4a\tilde{J}_1 (1-r)^2 k c_+} \left(\frac{\partial \mathbf{m}}{\partial \tau} \right)^2 + \frac{a}{4}\tilde{J}_1 c_+ \left(1 - \frac{c_-^2}{c_+^2} \right) \left(\frac{\partial \mathbf{m}}{\partial x} \right)^2 \right\}. \tag{15}$$

The first term is the topological term and θ is the topological angle given by

$$\theta = \frac{4\pi j(S_2 - rS_1)}{(1-r)(1+j) - kr}. \tag{16}$$

In the absence of frustration ($r=0$), the topological angle reduces to $\theta = 4\pi S_2 J_2/(J_1 + J_2)$. This is the same expression as that for a simple spin chain of magnitude S_2 with bond alternation.[10,12] This can be interpreted as follows: a spin $\mathbf{S}_1$ is combined with an adjacent spin $\mathbf{T}$ on the side chain, and a two-spin cluster with total spin magnitude $S_1 - T$ ($=S_2$) is formed. However, the coefficients of $(\partial\mathbf{m}/\partial\tau)^2$ and $(\partial\mathbf{m}/\partial x)^2$ in Eq. (15) do not reduce to those for the simple spin chain, even if k is very large. This implies that the quantum fluctuation of spins on side chains still survives for large k.

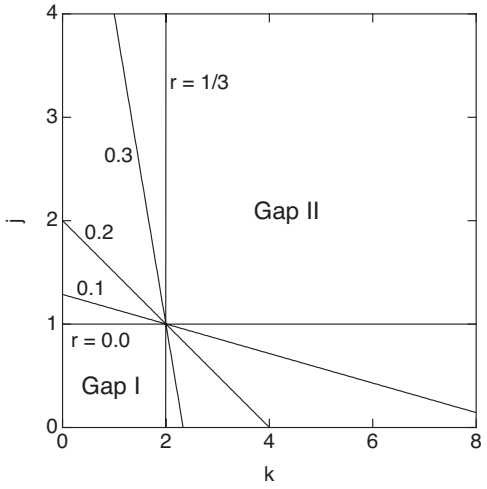

FIG. 2. Phase boundaries for several values of r in the k-j plane by the NLSM method for $S_1 = 1$, $S_2 = \frac{1}{2}$, and $T = \frac{1}{2}$. For each value of r ($=K_2/2K_1$), the region of $0 < k < \frac{1}{r} - 1$ is meaningful in the NLSM method.

The topological term of Eq. (15) determines whether or not the system has a spin gap in the same manner as Haldane's argument.[1] That is, the system does not have a spin gap if and only if the topological angle θ is just π (mod 2π). This condition is written as

$$\frac{2j(S_2 - rS_1)}{(1-r)(1+j) - kr} = h, \tag{17}$$

where h is any half odd integer. This gapless condition determines phase boundaries between gapful disordered phases in the parameter space. We notice that, for each value of h, boundaries for all values of r pass through the common point

$$(k, j) = \left(\frac{2(S_1 - S_2)}{2S_2 - h}, \frac{h}{2S_2 - h} \right). \tag{18}$$

In the case of $S_1 = 1$, $S_2 = \frac{1}{2}$, and $T = \frac{1}{2}$, only a permitted value of h in Eq. (17) is $\frac{1}{2}$ for $k > 0$ and $j > 0$. Then the phase boundaries for several values of r are solid lines in Fig. 2. Owing to the definitions of the parameters, they are straight lines in the present approximation. The regions of both sides of each boundary are gapful disordered phases. We call them Gap I phase and Gap II phase as noted in the figure. For $r=0$, the phase boundary is horizontal, since the topological angle is independent of k as mentioned below Eq. (16). This can be understood by considering $\mathbf{S}_1$ as a composite of two $\frac{1}{2}$ spins. In fact, when $r=0$, $\mathbf{T}$ and one of the $\frac{1}{2}$ spins of $\mathbf{S}_1$ necessarily form a valence bond irrespective of the value of k in the ground state. As r increases from 0, the slope of the boundary becomes negatively large. The reason will be argued later.

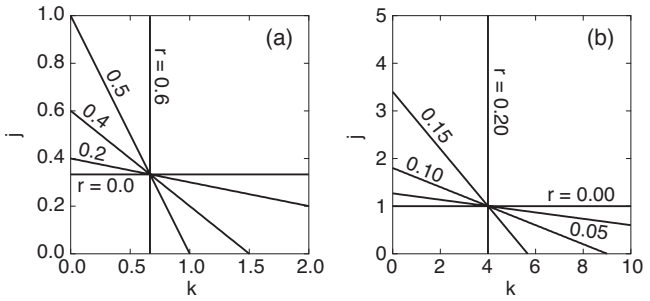

FIG. 3. Phase boundaries in the k-j plane by the NLSM method in the case of (a) $S_1=\frac{3}{2}$, $S_2=1$, and $T=\frac{1}{2}$, and (b) in the case of $S_1=\frac{3}{2}$, $S_2=\frac{1}{2}$, and $T=1$. For each value of r, the region of $0<k<\frac{1}{r}-1$ is meaningful.

We also show phase diagrams in other cases in Fig. 3; the phase boundaries in Fig. 3(a) are for $S_1=\frac{3}{2}$, $S_2=1$, and $T=\frac{1}{2}$, and those in Fig. 3(b) are for $S_1=\frac{3}{2}$, $S_2=\frac{1}{2}$, and $T=1$. Although Eq. (17), which determines the phase boundaries, is quite general, we mainly examine the case of $S_1=1$, $S_2=\frac{1}{2}$, and $T=\frac{1}{2}$. This case is expected to include the essence of the present type of spin chains with side chains.

IV. NUMERICAL DIAGONALIZATION

Hamiltonian (1) can be numerically diagonalized for small size systems. The numerical calculation is effective not only in analyzing the system itself in detail, but also in determining the precision of the NLSM method by comparing the results. We performed a numerical diagonalization in the case of $S_1=1$, $S_2=\frac{1}{2}$, and $T=\frac{1}{2}$ to obtain the phase diagram for the ground state.

The phase transition points are determined as follows. The phase transitions between different spin-gap phases are expected to be the Gaussian transition. Hence, we employ the method of twist boundary condition proposed by Kitazawa[13] and Kitazawa and Nomura[14] to determine the phase boundary. As will be examined later, the ground-state phases are described by different SCS configurations. Under the twisted boundary condition, the different singlet solid configurations have different time reversal parities depending on the even-odd parity of the number of valence bonds across the twisted boundary. Hence, the energy levels of the ground state and of the first excited state cross at the phase boundary without level repulsion. This ensures a precise evaluation of the phase boundary. The size extrapolation is based on the following formula for the finite size correction:[13,14]

$$j_c(N) = j_c(\infty) + \frac{c_1}{N^2} + \frac{c_2}{N^4}, \tag{19}$$

where $j_c(N)$ is the finite size critical value of quantity j, and c_1 and c_2 are the fitting parameters. We have carried out the extrapolation by using numerical results for the total spin number, $3N=12$, 18, and 24.

Resultant phase boundaries for several values of r are plotted in Fig. 4. By comparing Figs. 2 and 4, we find that the NLSM method gives qualitatively correct phase boundaries. In particular, for small r, or weak frustration, the

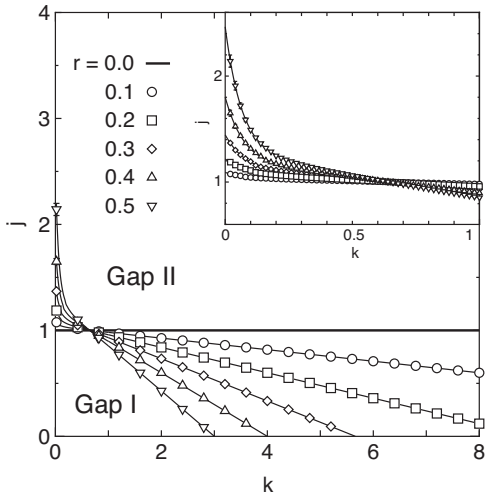

FIG. 4. Phase boundaries by numerical diagonalization for $S_1=1$, $S_2=\frac{1}{2}$, and $T=\frac{1}{2}$. Each point of a boundary is determined by extrapolation for the total spin number $3N=12$, 18, and 24. Inset: Phase boundaries for small k.

NLSM method provides a quantitatively fair approximation. With the increase in r, the Gap I phase extends to the region $j>1$ for small k, and it is suppressed in the region $j<1$ for large k. Although this feature qualitatively coincides with that of the NLSM results, quantitative coincidence becomes worse with the increase in r. This is natural because the present NLSM method starts from a classical antiferromagnetic solution in the absence of frustration.

The possibility of a first order transition between different spin-gap phases was pointed out in the frustrated ladder by Hakobyan *et al.*[15] in the appropriate parameter regime. By considering the presence of frustration, this type of transition cannot be ruled out in the present model. However, we did not find numerical evidence for the first order transition within the parameter regime discussed in this paper.

V. LIMITING CASES

To further confirm the numerical phase diagram for $S_1=1$, $S_2=\frac{1}{2}$, and $T=\frac{1}{2}$, we consider the effective theory in the limiting cases of $j\to 0$ and $j\to\infty$.

A. Strong J_1 limit ($j\to 0$)

In the limit of $j\to 0$, the system can be regarded as a one-dimensional array of weakly coupled three-spin units, as shown in Fig. 5(a). One of the three-spin units is described by the Hamiltonian

$$H_3 = J_1\mathbf{S}_1\cdot\mathbf{S}_2 + K_1\mathbf{S}_1\cdot\mathbf{T} + K_2\mathbf{S}_2\cdot\mathbf{T}, \tag{20}$$

where we have dropped the common index p representing the pth unit cell for simplicity. The Néel basis is represented as $|S_1^z, S_2^z, T^z\rangle$, where S_1^z takes $\Uparrow$, 0, or $\Downarrow$, and S_2^z and T take $\uparrow$ or $\downarrow$. By introducing the composed spin $\hat{\mathbf{S}}\equiv\mathbf{S}_1+\mathbf{S}_2+\mathbf{T}$, we have another set of basis vectors $||\tilde{S},\tilde{S}^z,\alpha\rangle\rangle$, where $\tilde{S}$ and $\tilde{S}^z$ are quantum numbers of the magnitude and the z component

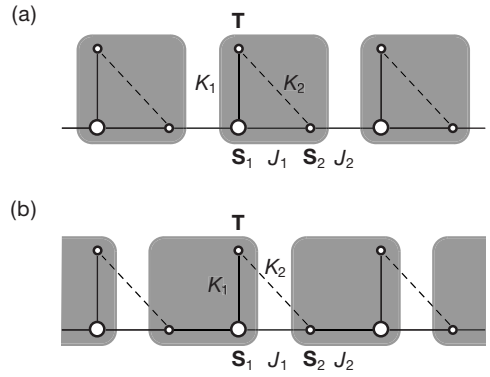

FIG. 5. (a) Three-spin units for $j \to 0$ and (b) those for $j \to \infty$ and $r \to 0$ in the case of $S_1=1$, $S_2=\frac{1}{2}$, and $T=\frac{1}{2}$. Three spins (circles) in a shadowed region form a three-spin unit.

of $\tilde{\mathbf{S}}$, respectively, and α discriminates multiple states with the same $\tilde{S}$ and $\tilde{S}^z$, if necessary. We seek the ground state of the three-spin unit with $\tilde{S}=0$ or 1, since all the exchange interactions are antiferromagnetic.

(i) For $\tilde{S}=0$, we have $\tilde{S}^z=0$. Then the one-dimensional subspace consists of a single state,

$$||0,0\rangle\rangle = \frac{1}{\sqrt{6}}(|0\downarrow\uparrow\rangle + |0\uparrow\downarrow\rangle - \sqrt{2}|\Uparrow\downarrow\downarrow\rangle - \sqrt{2}|\Downarrow\uparrow\uparrow\rangle). \tag{21}$$

This is a singlet eigenstate of H_3 belonging to the eigenvalue

$$E_0 = -J_1 - K_1 + \frac{K_2}{4}. \tag{22}$$

(ii) For $\tilde{S}=1$, we have $\tilde{S}^z=1$, 0, or -1. In this three-dimensional subspace, it is sufficient to inspect the case of $\tilde{S}^z=1$, owing to the spherical symmetry of the Hamiltonian H_3. We choose the orthonormal basis of the subspace $\tilde{S}=\tilde{S}^z=1$ as

$$||1,1,1\rangle\rangle = \frac{1}{2}(|\Uparrow\downarrow\uparrow\rangle + |\Uparrow\uparrow\downarrow\rangle - \sqrt{2}|0\uparrow\uparrow\rangle),$$

$$||1,1,2\rangle\rangle = \frac{1}{\sqrt{2}}(|\Uparrow\downarrow\uparrow\rangle - |\Uparrow\uparrow\downarrow\rangle). \tag{23}$$

By operating H_3 on these bases, we have an eigenvalue equation. Then the lowest eigenvalue E_1 in this subspace is determined as the smaller solution of the characteristic equation:

$$\begin{vmatrix} -\frac{J_1}{2} - \frac{K_1}{2} + \frac{K_2}{4} - E_1 & \frac{1}{\sqrt{2}}(-J_1 + K_1) \\ \frac{1}{\sqrt{2}}(-J_1 + K_1) & -\frac{3K_2}{4} - E_1 \end{vmatrix} = 0. \tag{24}$$

By introducing a normalized energy difference as $\epsilon=(E_1-E_0)/J_1$, Eq. (24) with Eq. (22) reduces to

$$2\epsilon^2 - [3(1+k) - 4rk]\epsilon + 2k[2 - (1+k)r] = 0. \tag{25}$$

If the smaller solution for ϵ is negative, the ground state is a triplet ($\tilde{S}=1$) state; otherwise, it is a singlet ($\tilde{S}=0$) state. By using Eq. (25), the condition for the triplet ground state becomes

$$k > k_c \equiv \frac{2}{r} - 1 \quad (\tilde{S}=1). \tag{26}$$

We notice that $k_c > 1$ in the region of $0<r<1$, which we have concentrated on in this paper. In the triplet ground state, $\mathbf{S}_2$ tends to orient to a direction opposite from $\mathbf{S}_1$ for $J_1>K_1$, and $\mathbf{T}$ does so for $J_1<K_1$. The composed spin $\tilde{\mathbf{S}}$ always orients in the same direction as $\mathbf{S}_1$.

The composed spin $\tilde{\mathbf{S}}(p)$ at the pth unit cell interacts with adjacent $\tilde{\mathbf{S}}(p+1)$ by an effective exchange interaction. We denote the effective exchange parameter by J_{eff}. Since the interaction between $\mathbf{S}_2(p)$ and $\mathbf{S}_1(p+1)$ is antiferromagnetic ($J_2>0$), the correlation between $\mathbf{S}_1(p)$ and $\mathbf{S}_1(p+1)$ is antiferromagnetic for $K_1>J_1$ ($k>1$) and ferromagnetic for $K_1<J_1$ ($k<1$). Therefore, J_{eff} has the same sign as $K_1-J_1=J_1(k-1)$, considering that the signs of $\langle\tilde{\mathbf{S}}(p)\cdot\tilde{\mathbf{S}}(p+1)\rangle$ and $\langle\mathbf{S}_1(p)\cdot\mathbf{S}_1(p+1)\rangle$ are the same.

For $k>k_c$, we have $J_{\text{eff}}>0$, since $k_c>1$ for $0<r<1$. Hence, the original spin chain is equivalent to a spin-1 antiferromagnetic Heisenberg chain consisting of effective spins, $\tilde{\mathbf{S}}(p)$'s. The ground state of a uniform spin-1 chain is the Haldane state,[1] which gives a spin gap for excitation. In the Haldane state, there is a strong correlation between each adjacent spin pair, as known from the VBS picture for effective spins, $\tilde{\mathbf{S}}(p)$'s.[7] In terms of the original spins, there is a strong correlation between adjacent three-spin units. For $k<k_c$, on the other hand, the ground state of each three-spin unit is already a closed singlet state. Then the ground state of the total spin chain is approximately an array of such closed local singlets, and there is almost no correlation between adjacent three-spin units. Thus, there is a Gaussian transition between the two characteristic ground states with spin gap at $k=k_c$. The value of k_c in this argument for $j \to 0$ agrees with the critical value by the numerical diagonalization, as seen on the $j=0$ line of the phase diagram (Fig. 4).

B. Strong J_2 limit ($j \to \infty$)

In the limit of $j \to \infty$, spins $\mathbf{S}_1(p+1)$ and $\mathbf{S}_2(p)$ form an effective spin $\hat{\mathbf{S}}(p) \equiv \mathbf{S}_1(p+1)+\mathbf{S}_2(p)$ with magnitude $\frac{1}{2}$, and other interactions can be treated as perturbations. Then the effective Hamiltonian for $\hat{\mathbf{S}}(p)$ and $\mathbf{T}(p)$ is

$$H_{\text{eff}} = \sum_{p=1}^{N} \left\{ -\frac{4}{9}J_1\hat{\mathbf{S}}(p)\cdot\hat{\mathbf{S}}(p+1) + \frac{4}{3}K_1\hat{\mathbf{S}}(p)\cdot\mathbf{T}(p+1) - \frac{1}{3}K_2\hat{\mathbf{S}}(p)\cdot\mathbf{T}(p) \right\}. \tag{27}$$

The ground state of this chain is still nontrivial. However, K_2 plays a secondary role in the weakly frustrated region, so that each $\mathbf{T}$ antiferromagnetically interacts with the ferromag-

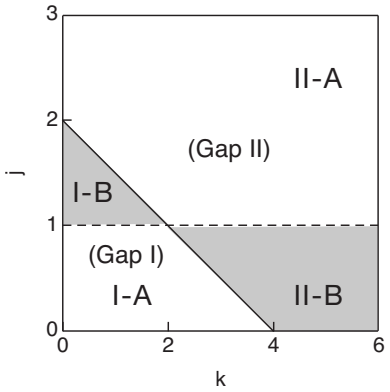

FIG. 6. Four regions in a typical phase diagram for $S_1=1$, $S_2=\frac{1}{2}$, and $T=\frac{1}{2}$; the phase diagram for $r=0.2$ by the NLSM method is shown. The solid line is the phase boundary between the Gap I phase and the Gap II phase. In each phase, the dashed line of $j=1$ means a crossover between regions with different features. The Gap I phase consists of regions I-A and I-B, while th Gap II phase consists of regions II-A and II-B. They are explained by SCS pictures.

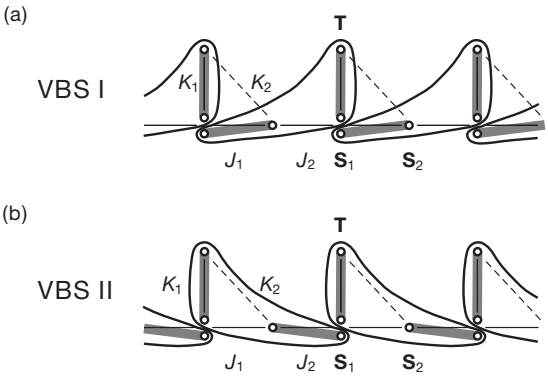

FIG. 7. VBS pictures in the limiting cases for $S_1=1$, $S_2=\frac{1}{2}$, and $T=\frac{1}{2}$: (a) VBS I represents the ground state for $j\to 0$ and $k<k_c$, and (b) VBS II does so for $j\to\infty$. Small circles are $\frac{1}{2}$ spins and bold gray lines are valence bonds. Spin $\mathbf{S}_1$ is expressed by two $\frac{1}{2}$ spins as $\mathbf{S}_1=\mathbf{S}_1^{(1)}+\mathbf{S}_1^{(2)}$. Loops including two valence bonds correspond to SCS pictures (see text).

netic chain consisting of $\hat{\mathbf{S}}$'s. Therefore, it is plausible that the ground state is always nonmagnetic for small r. Numerical studies of the effective model (27) suggest no phase transition for $0<r<1/3$, where no phase transition is predicted by the NLSM method for large j.

In terms of the original Hamiltonian (1), the ground state of $j\to\infty$ and $r\to 0$ is a direct product of local singlet states of three-spin units. A three-spin unit consists of $\mathbf{S}_2(p)$, $\mathbf{S}_1(p+1)$, and $\mathbf{T}(p+1)$, as shown in Fig. 5(b). The ground state of finite k and r $(j\to\infty)$ is adiabatically connected to the limit without phase transition as long as r is small. The full phase diagram of the effective model (27) is investigated in a separate paper.[16]

VI. SINGLET CLUSTER SOLID PICTURE

In this section, we propose the SCS picture to explain any ground state in the phase diagram for $S_1=1$, $S_2=\frac{1}{2}$, and $T=\frac{1}{2}$. This is a generalization of the VBS picture and is based on expressing $\mathbf{S}_1$ with a magnitude of 1 as

$$\mathbf{S}_1=\mathbf{S}_1^{(1)}+\mathbf{S}_1^{(2)}, \tag{28}$$

where $\mathbf{S}_1^{(1)}$ and $\mathbf{S}_1^{(2)}$ are spins with a magnitude of $\frac{1}{2}$.[17]

For convenience of explanation, we divide each phase into two regions by the line of $j=1$, as schematically shown in Fig. 6: the Gap I phase is divided into regions I-A and I-B, and the Gap II phase is divided into regions I-A and I-B.

A. Valence bond solid picture and its insufficiency

The ground states of the limiting cases in the preceding section are explained by VBS pictures. The VBS picture for $j\to 0$ and $k<k_c$ is VBS I, as illustrated in Fig. 7(a).[18] The valence bonds on J_1 interactions, which we hereafter abbreviate as the J_1 valence bonds, contribute mainly to the energy gain of the ground state of VBS I. On the other hand, the VBS picture for $j\to\infty$ is VBS II, as illustrated in Fig. 7(b). The valence bonds on J_2 interactions, or the J_2 valence bonds, contribute mainly to the energy gain of the ground state of VBS II.

The VBS pictures are not adequate for regimes away from the above limiting cases, although they are expected to be qualitatively valid for small-j and large-j regimes. As seen in Fig. 6, the energetic advantage of J_1 valence bonds of VBS I on line $j=0$ $(k<k_c)$ remains within region I-A because $J_1>J_2$. However, the advantage is lost in region I-B because $J_2>J_1$. Similarly, the energetic advantage of J_2 valence bonds of VBS II in the limit of $j\to\infty$ remains within region II-A because $J_2>J_1$. However, the advantage is lost in region II-B because $J_1>J_2$. Since the line of $j=1$ is not a phase boundary, we need a different picture to explain the whole Gap I (II) phase, which reduces to VBS I (II) in the limit. The picture will be a SCS picture.

B. Concept of a singlet cluster solid picture

A general SCS picture is defined by a wave function of a tensor product form of local singlet states. We call this wave function the SCS state, and each local singlet state a singlet cluster. It is typically written as

$$|\Psi\rangle=|\psi(1)\rangle\otimes|\psi(2)\rangle\cdots\otimes|\psi(M)\rangle, \tag{29}$$

where $|\psi(p)\rangle$ $(p=1,2,\ldots,M)$ is a singlet cluster and M is the total number of singlet clusters in the SCS state. Here, we have considered that any spin with a magnitude of more than 1 is resolved into a set of spins with a magnitude of $\frac{1}{2}$. Then a singlet cluster is a singlet state of more than two spins with a magnitude of $\frac{1}{2}$.

A singlet cluster in a SCS state is represented as a superposition of products of valence bonds. Hence, the valence bonds resonate within the singlet cluster. A VBS is a special case of the SCS, where a singlet cluster is a single valence bond and no resonation occurs. A resonating valence bond state is another special case, where the whole system is the singlet cluster and all valence bonds are resonating.

Usually, a SCS state is not the exact ground state for a given spin Hamiltonian. However, if the exact ground state is continuously modified into an appropriate SCS state, the SCS state describes the essence of the ground state. From this viewpoint, the SCS state is useful to characterize the phase to which the ground state belongs. In some quantum spin chains without a side chain, various ground-state phases have been successfully described by corresponding SCS pictures.[19] Furthermore, a SCS state can also quantitatively describe the true ground state if the wave function of each singlet cluster is well localized. Among such systems, in the spin system on a diamond chain,[20] we have the exact tetramer-dimer-state solution, which is a kind of SCS state.

C. Singlet cluster solid picture for the Gap I phase

We call the SCS picture for the Gap I phase SCS I. The SCS I state is constructed by assuming the following requirements:

(i) The ground state is continuously modified to the VBS I state without a global rearrangement of the valence bond configuration.
(ii) The ground state is invariant under the translation by a single unit cell.
(iii) The ground state contains a substantial amount of component with J_2 valence bonds in region I-B.

Assumption (i) is necessary, since the Gap I phase involves the limiting case of $j \to 0$ and $k < k_c$ where the VBS I picture holds, and there is no phase transition in the Gap I phase. As for assumption (ii), we confirmed that there is no indication of the translational symmetry breaking in numerical ground states. Assumption (iii) is required to explain region I-B.

Under the above requirements, we take the SCS I wave function in the tensor product form as follows:

$$|\Psi_{\mathrm{I}}(c)\rangle = |\psi_{\mathrm{I}}(1;c)\rangle \otimes |\psi_{\mathrm{I}}(2;c)\rangle \cdots \otimes |\psi_{\mathrm{I}}(N;c)\rangle, \quad (30)$$

as schematically depicted in Fig. 8(a). Here, $|\psi_{\mathrm{I}}(p;c)\rangle$ is a singlet cluster of four $\frac{1}{2}$ spins in the pth unit cell; this is denoted by a loop filled in gray. Each singlet cluster is a linear combination of two valence bond states written as

$$|\psi_{\mathrm{I}}(c)\rangle = |\alpha_{\mathrm{I}}\rangle + c|\beta_{\mathrm{I}}\rangle, \quad (31)$$

where $|\alpha_{\mathrm{I}}\rangle$ and $|\beta_{\mathrm{I}}\rangle$ are the valence bond states defined in the right hand side of Fig. 8(b). We have abbreviated index p of the unit cell for simplicity. The valence bond state $|\alpha_{\mathrm{I}}\rangle$ is the same as that shown within a loop in VBS I [Fig. 7(a)]. The valence bond state $|\beta_{\mathrm{I}}\rangle$ contains a J_2 valence bond. The coefficient c should be 0 in the limit of $j \to 0$ and may be small for region I-A ($J_1 > J_2$). However, it should have a substantial amplitude in region I-B ($J_1 < J_2$). For finite c, the two valence bond states locally resonate in a singlet cluster to contribute to energy gain; this effect is examined in Sec. VI E, where the phase boundary between the Gap I and Gap II phases is discussed energetically.

We examined which valence bonds really contribute to the ground state by numerically calculating the short range correlation functions. For a typical case ($r=0.3$ and $k=0.2$), results are shown in Fig. 9. As j increases, $|\langle \mathbf{S}_1(p)\cdot\mathbf{S}_2(p)\rangle|$ decreases and $|\langle \mathbf{S}_1(p+1)\cdot\mathbf{S}_2(p)\rangle|$ increases. This means that the contribution from the J_2 valence bonds becomes large in comparison with that from the J_1 valence bonds. It is also known that $|\langle \mathbf{S}_1(p)\cdot\mathbf{T}(p+1)\rangle|$ takes the maximum and $|\langle \mathbf{S}_1(p)\cdot\mathbf{T}(p)\rangle|$ takes the minimum around region I-B. Hence, a K_1 valence bond is reduced in region I-B. Instead, a valence bond between $\mathbf{T}(p+1)$ and $\mathbf{S}_1^{(1)}(p)$ [or $\mathbf{S}_1^{(2)}(p)$] develops, although there is no exchange interaction between $\mathbf{T}(p+1)$ and $\mathbf{S}_1(p)$. All these results are consistent with the SCS I picture.

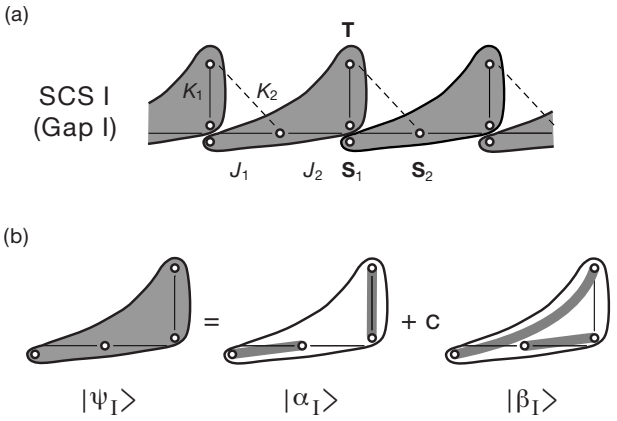

FIG. 8. (a) SCS I, the SCS picture for the Gap I phase ($S_1=1$, $S_2=\frac{1}{2}$, and $T=\frac{1}{2}$). SCS I is a tensor product form of singlet clusters. (b) A singlet cluster $|\psi_{\mathrm{I}}(c)\rangle$ (the left hand side) in SCS I. It is represented as a linear combination of two valence bond states, $|\alpha_{\mathrm{I}}\rangle$ and $|\beta_{\mathrm{I}}\rangle$ (the right hand side). c is the coefficient of the linear combination.

D. Singlet cluster solid picture for the Gap II phase

We call the SCS picture for the Gap II phase SCS II. Similar to the case of SCS I, the SCS II state is constructed by assuming the following requirements:

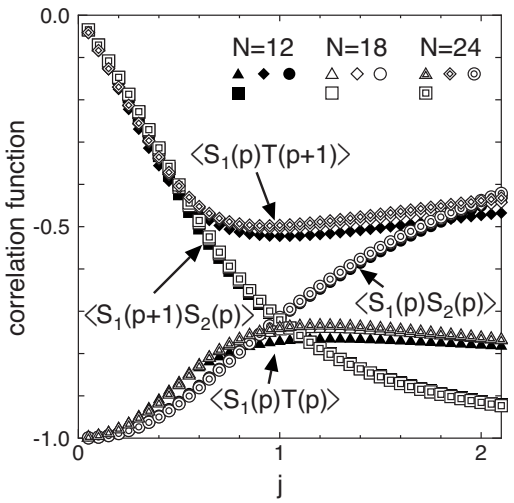

FIG. 9. Short range correlation functions for $r=0.3$ and $k=0.2$ numerically calculated for $N=12$, 18, and 24 (N is the number of spins).

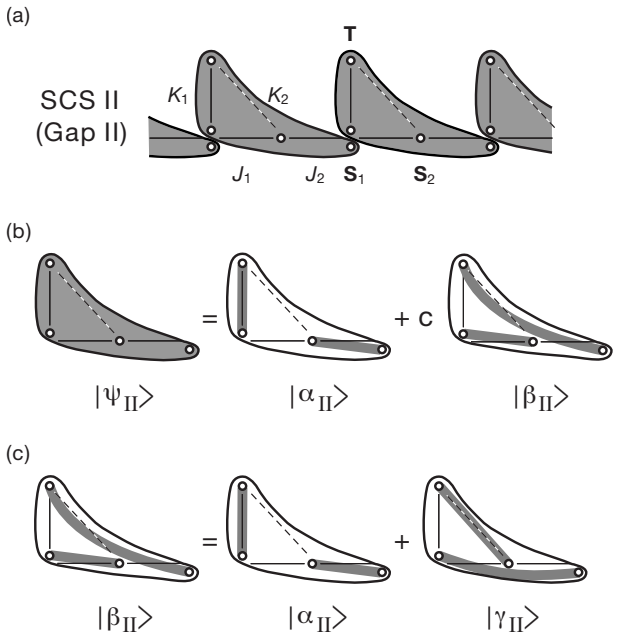

FIG. 10. (a) SCS II, the SCS picture for the Gap II phase ($S_1=1$, $S_2=\frac{1}{2}$, and $T=\frac{1}{2}$). SCS II is a tensor product form of singlet clusters. (b) A singlet cluster $|\psi_{II}(c)\rangle$ (the left hand side) in SCS II. It is represented as a linear combination of two valence bond states, $|\alpha_{II}\rangle$ and $|\beta_{II}\rangle$ (the right hand side). c is the coefficient of the linear combination. (c) Identity among local valence bond states. $|\beta_{II}\rangle$ (the left hand side) is exactly the sum of $|\alpha_{II}\rangle$ and $|\gamma_{II}\rangle$ (the right hand side).

(i) The ground state is continuously modified to the VBS II state without a global rearrangement of the valence bond configuration.

(ii) The ground state is invariant under the translation by a single unit cell.

(iii) The ground state contains a substantial amount of component with J_1 valence bonds in region II-B.

Under the above requirements, we take the SCS II wave function in the tensor product form

$$|\Psi_{II}(c)\rangle = |\psi_{II}(1;c)\rangle \otimes |\psi_{II}(2;c)\rangle \cdots \otimes |\psi_{II}(N;c)\rangle, \quad (32)$$

as schematically depicted in Fig. 10(a). Here, $|\psi_{II}(p)\rangle$ is a singlet cluster of four $\frac{1}{2}$ spins in the pth unit cell; this is denoted by a loop filled in gray. Each singlet cluster is a linear combination of two valence bond states written as

$$|\psi_{II}(c)\rangle = |\alpha_{II}\rangle + c|\beta_{II}\rangle, \quad (33)$$

where $|\alpha_{II}\rangle$ and $|\beta_{II}\rangle$ are the two valence bond states defined in the right hand side of Fig. 10(b). We have abbreviated index p of the unit cell for simplicity. The valence bond state $|\alpha_{II}\rangle$ is the same as that shown within a loop in VBS II [Fig. 7(b)]. The valence bond state $|\beta_{II}\rangle$ contains a J_1 valence bond. The coefficient c should be 0 in the limit of $j\to\infty$ and may be small for region II-A ($J_1<J_2$). However, it should have substantial amplitude in region II-B ($J_1>J_2$). For finite c, the two valence bond states locally resonate in a singlet cluster to contribute to energy gain; this effect is examined in Sec. VI E.

The wave function (33) of the singlet cluster is also represented as

$$|\psi_{II}(c)\rangle = (1+c)|\alpha_{II}\rangle + c|\gamma_{II}\rangle \quad (34)$$

by using the identity $|\beta_{II}\rangle = |\alpha_{II}\rangle + |\gamma_{II}\rangle$, which is shown in Fig. 10(c). $|\gamma_{II}\rangle$ includes the valence bond on the K_2 interaction and contributes to energy gain in region II-B ($K_2 \gg K_1$).

E. Boundary between Gap I and Gap II phases

First, we consider the $j>1$ part of the phase boundary; it separates regions I-B and II-A, as seen in Fig. 6. The SCS II wave function in region II-A is close to VBS II with J_2 valence bonds, while the SCS I wave function in region I-B contains J_2 valence bonds only partly in the linear combination [Eq. (31)]. Then, since the energy gain owing to J_2 valence bonds in region II-A is always larger than that in region I-B, one might expect that region II-A would extend to the whole area of $j>1$. The reason why region I-B actually exists is attributed to the energy gain by local resonation between the two valence bond states within each singlet cluster [Eq. (31)]. When k or j increases, the SCS I becomes less favorable and VBS II becomes advantageous because of strong K_1 or J_2 valence bonds.

Second, we consider the $j<1$ part of the phase boundary; it separates regions II-B and I-A, as seen in Fig. 6. The SCS I wave function in region I-A is close to VBS I with J_1 valence bonds, while the SCS II wave function in region II-B contains J_1 valence bonds only partly in the linear combination [Eq. (33)]. Then, since the energy gain owing to J_1 valence bonds in region I-A is always larger than that in region II-B, one might expect that region I-A would extend to the whole area of $j<1$. The reason why region II-B actually exists is attributed to the energy gain by local resonation between the two valence bond states within each singlet cluster [Eq. (33)]. Since the resonation is enhanced by the frustration due to K_2 interactions, the area of region I-B increases with increasing r ($=K_2/2K_1$), as seen in Figs. 2 and 4. If r is fixed, the increase in k ($=K_1/2J_1$) diminishes the effect of J_1 interactions and makes the effect of resonation in SCS II advantageous. This is the reason why SCS II appears for a relatively large k in the presence of frustration r.

VII. VARIATIONAL CALCULATION

In the preceding section, we explained that the SCS picture represents the essence of each ground-state phase. However, it does not guarantee that each SCS wave function is quantitatively satisfactory. In this section, we perform variational calculation using the SCS I and SCS II wave functions to examine the quantitative correctness of the wave functions.

A. Variational calculation for SCS I

The variational wave function for SCS I is Eq. (30) with variational parameter c, which is the coefficient of the linear

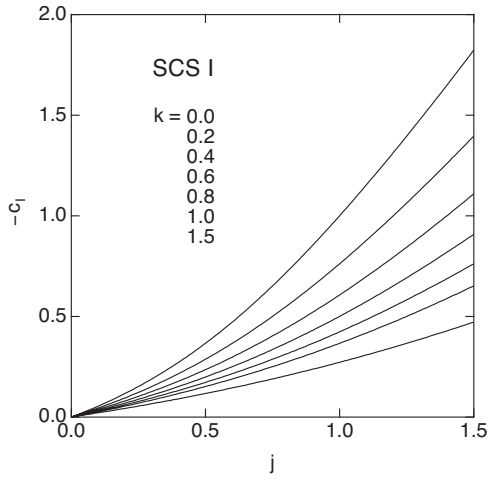

FIG. 11. Coefficient c_I of the linear combination in the variational wave function for SCS I ($S_1=1$, $S_2=\frac{1}{2}$, and $T=\frac{1}{2}$). The optimal coefficient c does not depend on r in the wave function. The lines are in the order of ascending k from top to bottom.

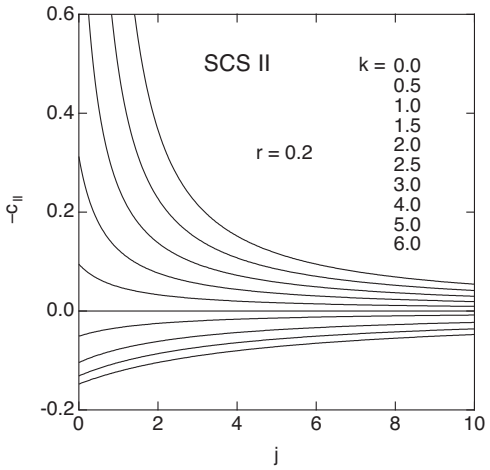

FIG. 12. Coefficient c_{II} of the linear combination in the variational wave function for SCS I in the case of $r=0.2$ ($S_1=1$, $S_2=\frac{1}{2}$, and $T=\frac{1}{2}$). The lines are in the order of ascending k from top to bottom.

combination. Then the energy per unit cell in energy unit J_1 is written as

$$\epsilon_I(c) = \frac{1}{NJ_1}\frac{\langle\Psi_I(c)|H|\Psi_I(c)\rangle}{\langle\Psi_I(c)|\ \Psi_I(c)\rangle} = \frac{\langle\psi_I(c)|h_I|\psi_I(c)\rangle}{\langle\psi_I(c)|\ \psi_I(c)\rangle}, \quad (35)$$

where H is the total Hamiltonian (1), and h_I is the reduced Hamiltonian for a singlet cluster in SCS I given as

$$h_I = \mathbf{S}_1^{(1)} \cdot \mathbf{S}_2 + j\mathbf{S}_2 \cdot \mathbf{S}_1^{(2)} + k\mathbf{S}_1^{(2)} \cdot \mathbf{T}. \quad (36)$$

After a straightforward calculation, we have the following formula:

$$\epsilon_I(c) = -\frac{3}{4}\frac{1+k-(1+k+j)c+jc^2}{1-c+c^2}. \quad (37)$$

By minimizing $\epsilon_I(c)$ with respect to c, we have the optimal value c_{II} of the coefficient of the linear combination

$$c_I = \frac{1+k-j-\sqrt{(1+k)^2-(1+k)j+j^2}}{1+k}. \quad (38)$$

The result is shown in Fig. 11, where the left axis represents $-c_I$. It is independent of r, since a K_2 interaction is between different singlet clusters. In the limit of $j\to 0$, we have $c_I=0$ and the wave function reduces to VBS I. The value $|c_I|$ increases with increasing j, and for $j\gtrsim 1$, the term of $|\beta_I\rangle$ including J_2 valence bonds becomes dominant in $|\psi_I(c)\rangle$. This behavior is consistent with the argument about SCS I in the preceding section.

B. Variational calculation for SCS II

The variational wave function for SCS II is Eq. (32) with variational parameter c, which is the coefficient of the linear combination. Then the energy per unit cell in energy unit J_1 is written as

$$\epsilon_{II}(c) = \frac{1}{NJ_1}\frac{\langle\Psi_{II}(c)|H|\Psi_{II}(c)\rangle}{\langle\Psi_{II}(c)|\ \Psi_{II}(c)\rangle} = \frac{\langle\psi_{II}(c)|h_{II}|\psi_{II}(c)\rangle}{\langle\psi_{II}(c)|\ \psi_{II}(c)\rangle}, \quad (39)$$

where H is the total Hamiltonian (1), and h_{II} is the reduced Hamiltonian for a singlet cluster in SCS II given as

$$h_{II} = k\mathbf{T} \cdot \mathbf{S}_1^{(2)} + \mathbf{S}_1^{(2)} \cdot \mathbf{S}_2 + j\mathbf{S}_2 \cdot \mathbf{S}_1^{(1)} + 2kr\mathbf{T} \cdot \mathbf{S}_2. \quad (40)$$

After a straightforward calculation, we have the following formula:

$$\epsilon_{II}(c) = -\frac{3}{4}\frac{j+k-(1+k+j-2kr)c+c^2}{1-c+c^2}. \quad (41)$$

By minimizing $\epsilon_{II}(c)$ with respect to c, we have the optimal value c_{II} of the coefficient of the linear combination as follows:

$$c_{II} = \frac{a-\sqrt{a^2+ab+b^2}}{a+b} \quad (42)$$

with $a=j+k-1$ and $b=1-2kr$. The result for $r=0.2$ is shown in Fig. 12, where the left axis represents $-c_{II}$. In the limit of $j\to\infty$, we have $c_{II}=0$ and the wave function reduces to VBS II.

The result depends on r, since a K_2 interaction is involved in each singlet cluster. Except for $r=1/2k$, $|c_{II}|$ increases with decreasing j, which means that $|\beta_{II}\rangle$ including J_1 valence bonds becomes dominant in Eq. (33). This feature is consistent with the SCS II picture in the preceding section. In the special case of $2kr$ $(=K_2/J_1)=1$, we have $c_{II}=0$ for any values of j, since $b=0$ in Eq. (42). It is explained in the following expression for $|\psi_{II}(c)\rangle$:

$$|\psi_{II}(c)\rangle = (1+c)|\beta_{II}\rangle - |\gamma_{II}\rangle, \quad (43)$$

which is derived from Eq. (33) by the identity $|\beta_{II}\rangle=|\alpha_{II}\rangle+|\gamma_{II}\rangle$ in Fig. 10(c). For $J_1=K_2$, $|\beta_{II}\rangle$ with a J_1 valence bond and $|\gamma_{II}\rangle$ with a K_2 valence bond are equally weighted in Eq. (43), as expected.

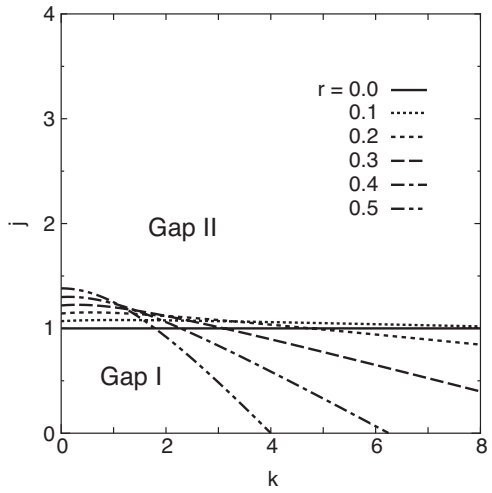

FIG. 13. Phase boundaries by the variational calculation for the SCS wave functions ($S_1=1$, $S_2=\frac{1}{2}$, and $T=\frac{1}{2}$).

C. Phase diagram by variational calculation

In the above sections, we have obtained the variational energy $\epsilon_{\mathrm{I}}(c_{\mathrm{I}})$ of SCS I for the Gap I phase and the variational energy $\epsilon_{\mathrm{II}}(c_{\mathrm{II}})$ of SCS II for the Gap II phase. The phase boundary is determined by the equation

$$\epsilon_{\mathrm{I}}(c_{\mathrm{I}}) = \epsilon_{\mathrm{II}}(c_{\mathrm{II}}). \tag{44}$$

The results for various r are shown in Fig. 13. These phase boundaries qualitatively agree with the numerical ones in Fig. 4 and support the correctness of the SCS pictures.

Region I-B in the variational phase diagram is wider in the k direction and narrower in the j direction than that in the accurate one (Fig. 4). Further, region II-B is narrower than the accurate one. By remembering that regions I-B and II-B exist because of the local resonation of valence bond states, the inclusion of longer range valence bonds resonating with each other is possibly effective in improving the variational wave functions in regions I-B and II-B. The ground states in regions I-A and II-A are close to VBS I and VBS II, respectively, and the effect of resonation is relatively small. Hence, the inclusion of longer range valence bonds does not seem to be very effective in improving the variational wave functions.

VIII. SUMMARY AND DISCUSSION

In this paper, we investigated the nonmagnetic ground states of a mixed spin chain with side chains with weak frustration. So far, these kinds of models have not been investigated in depth despite their possible rich physics. We have chosen the present model (1) (Fig. 1) as a simple and nontrivial one, which will be a good starting point. We examined the system in various approaches: a NLSM method, a numerical diagonalization method, an inspection of limiting cases, a physical interpretation based on SCS pictures, and a variational calculation for SCS wave functions.

NLSM methods have been developed for simple spin chains without a side chain. In the present work, we formulated a NLSM method for the typical spin chain with side chains. The NLSM method analytically provides a ground-state phase diagram in the k-j parameter space for various values of S_1, S_2, and T. In the special case of $S_1=1$, $S_2=\frac{1}{2}$, and $T=\frac{1}{2}$, the phase diagram contains two quantum disordered phases, Gap I and Gap II, in each of which the system has a spin gap.

We also examined the case of $S_1=1$, $S_2=\frac{1}{2}$, and $T=\frac{1}{2}$ by the numerical diagonalization for finite chains. By using the method of twisted boundary condition, we have determined phase boundaries. When frustration is not strong ($r\lesssim 1$), there are two spin-gap phases in the k-j parameter space. The numerical results confirm the qualitative correctness of the present NLSM method.

The limiting cases of $j\to 0$ and $j\to\infty$ are precisely and analytically treated. For $j\ll 1$, the Hamiltonian (1) describes an array of weakly coupled three-spin units. As k increases from 0, the ground state of each three-spin unit changes from singlet to triplet. Accordingly, the whole spin chain undergoes a phase transition from the VBS I state to the Haldane state. For $j\gg 1$, the system is described by an effective Hamiltonian where no phase transition occurs with changing k as long as r is small. By considering the continuity to the large k limit, the ground state is described as a state similar to the VBS II state.

There are regimes where no VBS picture explains the ground state for $S_1=1$, $S_2=\frac{1}{2}$, and $T=\frac{1}{2}$. To explain the whole phase diagram, we proposed two SCS pictures: SCS I and SCS II for Gap I and Gap II phases, respectively. Each SCS is a wave function of a tensor product form of singlet clusters. A singlet cluster in both the SCS states is a local linear combination of two valence bond states of two different patterns. The resonation contributes to the energy gain of the system and whole phases are consistently explained.

To quantify the SCS pictures, we performed variational calculations with the wave functions representing SCS I and SCS II. The phase boundary between the Gap I and Gap II phases is determined by equating the energy of the minimized wave function for SCS I to that for SCS II. The resultant phase diagram approximately reproduces the phase diagram by the numerical diagonalization.

Thus, we have obtained three phase diagrams: Fig. 2 by the NLSM method, Fig. 4 by the numerical diagonalization, and Fig. 13 by the variational calculation. The phase diagram of Fig. 4 is accurate, since the extrapolation by finite size systems is reliable. The other phase diagrams qualitatively agree with the accurate one, and both methods are shown to be useful.

So far, we have examined the spin chain with side chains when the parameter r measuring frustration is not large ($r\lesssim 1$). For larger r, a wider variety of phases is expected. For example, we can extend the analysis in the limit of $j\to 0$ to the region of $r>1$, i.e., $k_c<1$. For $k_c<k<1$, effective spins of three-spin units with a spin magnitude of 1 ferromagnetically interact with the nearest neighbors and form a ferromagnetic ground state. In terms of the original spins, the ground state is ferrimagnetic. Further, by the numerical diagonalization, we have found various ferrimagnetic phases with different magnetization in the strongly

frustrated regime. The study of these ferrimagnetic phases is in progress and will be reported in a separate paper.

ACKNOWLEDGMENTS

The numerical diagonalization program is based on the package TITPACK Version 2 coded by H. Nishimori. The numerical computation in this work was carried out by using the facilities of the Supercomputer Center, Institute for Solid State Physics, University of Tokyo and Information Technology Center, University of Tokyo. This work is partly supported by Fund for Project Research in Toyota Technological Institute and by Innovative Research Organization, Saitama University.

[1] F. D. M. Haldane, Phys. Rev. Lett. **50**, 1153 (1983); Phys. Lett. **93A**, 464 (1983).

[2] M. C. Cross and D. S. Fisher, Phys. Rev. B **19**, 402 (1979); J. L. Black and V. J. Emery, *ibid.* **23**, 429 (1981); T. Nakano and H. Fukuyama, J. Phys. Soc. Jpn. **49**, 1679 (1980); K. Hida, Phys. Rev. B **45**, 2207 (1992).

[3] S. P. Strong and A. J. Millis, Phys. Rev. Lett. **69**, 2419 (1992); Phys. Rev. B **50**, 9911 (1994); T. Barnes, E. Dagotto, J. Riera, and E. S. Swanson, *ibid.* **47**, 3196 (1993); K. Hida, J. Phys. Soc. Jpn. **64**, 4896 (1995); K. Totsuka and M. Suzuki, J. Phys.: Condens. Matter **7**, 6079 (1995); T. Narushima, T. Nakamura, and S. Takada, J. Phys. Soc. Jpn. **64**, 4322 (1995).

[4] S. Doniach, Physica B & C **91**, 231 (1977).

[5] R. T. Scalettar, D. J. Scalapino, and R. L. Sugar, Phys. Rev. B **31**, 7316 (1985); H. Otsuka and T. Nishino, *ibid.* **52**, 15066 (1995); Y. Chen, Q. Yuan, H. Chen, and Y. Zhang, Phys. Lett. A **245**, 167 (1998).

[6] A. Honecker and W. Brenig, Phys. Rev. B **63**, 144416 (2001); V. R. Chandra, D. Sen, N. B. Ivanov, and J. Richter, *ibid.* **69**, 214406 (2004); S. Chen, Y. Wang, W. Q. Ning, C. Wu, and H. Q. Lin, *ibid.* **74**, 174424 (2006).

[7] I. Affleck, T. Kennedy, E. H. Lieb, and H. Tasaki, Phys. Rev. Lett. **59**, 799 (1987).

[8] For example, see J. S. Miller, Inorg. Chem. **39**, 4392 (2000); *Magnetism: Molecules to Materials II, Molecule-Based Materials*, edited by J. S. Miller and M. Drillon (Wiley-VCH, Weinheim, 2001); *Carbon-Based Magnetism: An Overview of the Magnetism of Metal Free Carbon-Based Compounds and Materials*, edited by T. L. Makarova and F. Palacio (Elsevier, Amsterdam, 2006).

[9] The model is also considered as a spin chain with first neighbor couplings K_1, K_2 and J_2, and second neighbor coupling J_1.

[10] K. Takano, Phys. Rev. Lett. **82**, 5124 (1999).

[11] One among $\mathbf{L}_1$, $\mathbf{L}_2$ and $\mathbf{L}_\perp$ is a dummy variable. It is absorbed by the others, and only two variables remain, as seen in Eq. (12). Hence, the number of the original degrees of freedom is conserved.

[12] I. Affleck, Nucl. Phys. B **257**, 397 (1985); **265**, 409 (1986).

[13] A. Kitazawa, J. Phys. A **30**, L285 (1997).

[14] A. Kitazawa and K. Nomura, J. Phys. Soc. Jpn. **66**, 3944 (1997).

[15] T. Hakobyan, J. H. Hetherington, and M. Roger, Phys. Rev. B **63**, 144433 (2001).

[16] K. Hida, arXiv:0709.1423, J. Phys. Soc. Jpn. (to be published 2008).

[17] For the equivalence, $\mathbf{S}_1^{(1)}$ and $\mathbf{S}_1^{(2)}$ are symmetrized in a wave function.

[18] The wave function (21) for a three-spin unit is expressed as $||0,0\rangle\rangle=(|\mathbf{S}_1^{(1)}\mathbf{T}\rangle|\mathbf{S}_1^{(2)}\mathbf{S}_2\rangle+|\mathbf{S}_1^{(2)}\mathbf{T}\rangle|\mathbf{S}_1^{(1)}\mathbf{S}_2\rangle)/\sqrt{2}$, where $|\mathbf{SS}'\rangle$ means the valence bond state between $\mathbf{S}$ ($=\mathbf{S}_1^{(1)}$ or $\mathbf{S}_1^{(2)}$) and $\mathbf{S}'$ ($=\mathbf{S}_2$ or $\mathbf{T}$). This is part of VBS I in Fig. 7(a).

[19] K. Takano, Phys. Rev. B **61**, 8863 (2000); Physica B (Amsterdam) **284-288**, 1555 (2000); J. Phys. Chem. Solids **62**, 377 (2001).

[20] K. Takano, K. Kubo, and H. Sakamoto, J. Phys.: Condens. Matter **8**, 6405 (1996).